Open Access   Original Article

Sodium alginate/κ-carrageenan films for mupirocin dermal delivery

Tamara Rodrigues de Sousa[1], Sayza Dias de Santana[2], Grasiele Soares Cavallini[1,2] , Nelson Luis Gonçalves Dias de Souza[1,2]*

[1]Chemistry Department, Postgraduate Program in Chemistry, Federal University of Tocantins, Gurupi 77410-530, Brazil
[2]Chemistry Department, Federal University of Tocantins, Gurupi 77410-530, Brazil

*Correspondence: Nelson Luis Gonçalves Dias de Souza, Chemistry Department, Federal University of Tocantins, Gurupi 77410-530, Brazil. nelson.luis@uft.edu.br

Abstract

Aim: The chronicity of injuries is also a public health problem, and it is necessary to develop and apply new materials to promote more satisfactory results in the wound healing. Thus, this study aims to develop natural polymer films based on a combination of κ-carrageenan and sodium alginate, crosslinked with Zn^{2+}, for the controlled delivery of mupirocin (MUP).

Methods: Vibrational spectroscopy (Raman and infrared spectroscopies) was used to characterize the chemical structure and crosslinking process. Micro-Raman imaging and scanning electron microscopy were employed to observe the spatial distribution of the polymers and morphology of the samples, respectively. The uniformity (in terms of mass, thickness, and MUP concentration) of the films, MUP release kinetics, and their bactericidal activity were subjected to analysis.

Results: The films exhibited good uniformity in terms of thickness, mass, and quantity of MUP. However, the percentage of antibiotics was lower than that added, indicating losses during the film production process. Swelling and release kinetic studies indicated good swelling capacity of the films and controlled drug delivery process. The antibacterial activity of the films was determined against *Staphylococcus aureus*, *Escherichia coli*, *Staphylococcus epidermidis*, and *Pseudomonas aeruginosa* using the zone of inhibition method. All films produced showed activity against the growth of these bacteria.

Conclusions: The results illustrate the potential of employing κ-carrageenan and sodium alginate in the fabrication of polymeric films for the regulated release of MUP, with the aim of developing wound dressings that can improve wound healing outcomes.

Keywords

Carbohydrate, antibiotic, wounds, controlled delivery

Introduction

Wound healing remains a problem because wounds caused by burns, chronic diseases, trauma, and post-surgery may be unavoidable for the proliferation of resistant microorganisms [1]. Thus, skin repair is indispensable, and the faster it occurs, the shorter the exposure time of the body to a series of pathogens [2]. Chronic wounds, which do not heal easily and generate a vicious cycle of inflammation and infection, impair the functional restoration of skin tissue [3].

Studies indicate that patients with chronic wounds have an affected quality of life compared to those who are not affected because of pain, difficulty in walking, dissatisfaction, anxiety, depression, social isolation, and constantly changing body image, causing a decrease in self-esteem and functional ability, and often preventing them from carrying out their routine activities [4–6].

Successful treatment of chronic wounds involves several factors, and complications, such as preexisting diseases, comorbidities, and advanced age, can make this process difficult. One such treatment is the use of topical antibiotics [7]. Mupirocin (MUP), a class of antibiotics used to treat wounds, inhibits the synthesis of bacterial proteins by the reversible and specific binding of isoleucyl tRNA synthetase [8]. It has excellent activity against gram-positive staphylococci, but its activity against gram-negative organisms is more variable [9].

Although MUP is used to treat various bacterial skin infections, it has some limitations such as a short half-life, high protein binding, and drug resistance. Therefore, new strategies for its administration have been adopted to improve patient safety, reduce drug resistance, and expand its delivery [10].

In recent years, polymer-based films have been developed as a means of sustained or controlled drug delivery, with adhesive properties, providing the drug to a specific location on the skin in a prolonged manner, and improving therapeutic effects [11]. Among polymers, hydrogels have the advantage of maintaining the environment hydrated and ideal for treatment, in addition to having low interfacial tension, high permeability to oxygen and water, absorption of excess exudates, easy trauma, and good mechanical properties [12, 13]. Particularly, carbohydrate-based hydrogels are good candidates for the construction of delivery systems because they are nontoxic, biocompatible, and biodegradable [14].

The novelty of our study was the production of biodegradable films based on sodium alginate and κ-carrageenan, loaded with MUP, which exhibited antibacterial activities against both gram-positive and gram-negative microorganisms. Films comprising different proportions of the polysaccharides were obtained through crosslinking with the Zn^{2+} ion and were applied as a matrix for the controlled delivery of MUP. Zn^{2+} was selected as the crosslinking agent because it is an essential micronutrient for human health with significant biological relevance and abundance in the epidermis. Topical zinc sulfate has also been used to treat wounds and improve healing [15]. The obtained films were characterized by infrared spectroscopy, Raman spectroscopy, micro-Raman imaging, and scanning electron microscopy (SEM). The degree of swelling, uniformity, release, permeation kinetics, and antimicrobial effects of the films against the four bacteria were studied.

Materials and methods

Film preparation

The polymer films were prepared using the solvent casting method [1, 16]. First, 20 mL of an aqueous solution containing 5% *w/v* of the polymers (sodium alginate/κ-carrageenan) and 0.08 g of MUP (8% in relation to the polymer mass) was prepared and stirred for 4 h. The solutions were thereafter poured into Petri dishes for solvent evaporation at room temperature (25–28°C). After drying, the obtained films were immersed in 20 mL of 1.0% *w/v* zinc acetate aqueous solution for 5 min to perform the crosslinking process (Figure 1). The films were washed with excess distilled water and dried at room temperature. The obtained polymeric films and their compositions are listed in Table 1 and for comparative purposes, samples without the crosslinking process were obtained.
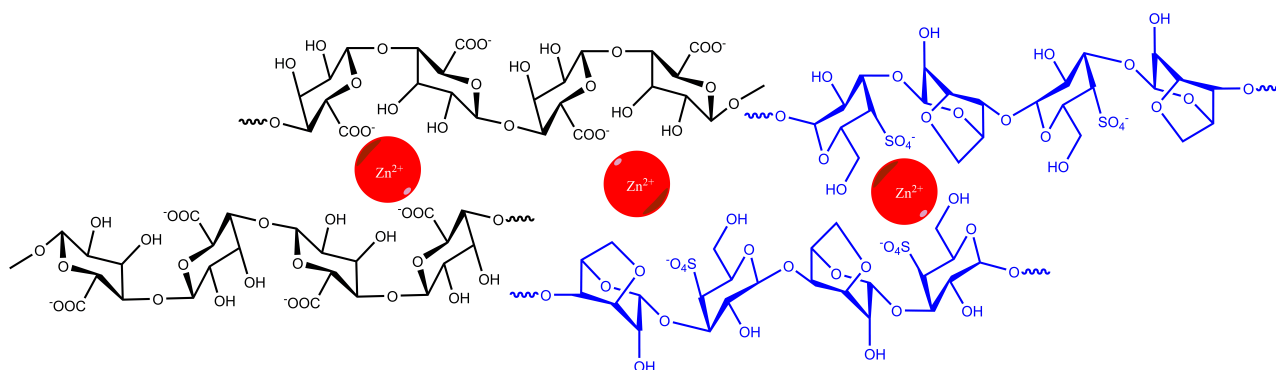
— Sodium alginate

— κ-carrageenan

Figure 1. Crosslinking of sodium alginate/κ-carrageenan with Zn^{2+}

Table 1. The composition of polymer films is expressed as a percentage in relation to mass

Films	Sodium alginate (%)	κ-carrageenan (%)	Crosslinking
F1	50	50	Present
F2	75	25	Present
F3	25	75	Present
F4	50	50	Absent
F5	75	25	Absent
F6	25	75	Absent

Swelling

The water absorption study was conducted using five circles of each film with a diameter of 6 mm, obtained using a paper punch. Initially, the mass of each dry sample was checked and thereafter left to rest in a pH 7 phosphate buffer solution with 5% methanol. At certain times, the films were removed from the solution, excess moisture was removed with a paper towel, and the mass was measured and submerged in phosphate buffer pH 7 with 5% methanol again to continue the swelling evaluation.

Uniformity tests of polymer films (thickness, mass, and MUP concentration)

To perform the tests, the obtained films were perforated with the aid of a paper punch to generate circular pieces of film with a diameter of 6 mm. Thus, to achieve uniformity in thickness, the thickness of five pieces of each film was measured, with the aid of a caliper. To ensure mass uniformity, the mass of five pieces of each film was measured using an analytical balance. The MUP content test was performed by immersing five pieces of each film in 10 mL of an aqueous solution of phosphate buffer (pH 7.4) and methanol in a ratio of 3:1, respectively, for 24 h. After this period, the obtained solution was filtered, and the MUP concentration was measured at 226 nm using a PG Instruments T70 ultraviolet-visible (UV-vis) spectrophotometer [8].

Permeation and release kinetics

In vitro MUP permeation and release studies were performed in duplicate using the Franz cell method. The formulation under study was added to the donor compartment, and over time, an aliquot was removed from the recipient compartment to quantify the MUP using UV-vis spectroscopy at a wavelength of 226 nm. As MUP transport medium, an aqueous phosphate buffer solution (pH 7.4) with 5% methanol and a polysulfone membrane were used as the interface between the donor and receptor compartments. The obtained data were adjusted to zero-order, first-order, Higuchi, Korsmeyer-Peppas, and Weibull models [17–19].

In vitro microbiological test—polymer disc diffusion test

A disk diffusion sensitivity test was performed to evaluate the antimicrobial activities of the polymer films. For the positive control, 200 μg of MUP was used and the negative control was sterile distilled water. The microorganisms used in the bioassay were extracted from standard strains (American Type Collection Culture-ATCC) of gram-positive bacteria, *Staphylococcus aureus* (ATCC 6538) and *Staphylococcus epidermidis* (ATCC 0128), and gram-negative bacteria, *Escherichia coli* (ATCC 25922) and *Pseudomonas aeruginosa* (ATCC 27893), recommended for antimicrobial susceptibility testing and associated with skin wounds [20].

The ATCC strains of microorganisms were activated by seeding in 90 mm Petri dishes containing Cromoclin US Agar medium and stored in a bacteriological oven at 37°C for 24 h. After 24 h, the microorganisms on the plates were manipulated, and each inoculum was transferred to a test tube containing sterile saline solution. The turbidity obtained using this dilution was adjusted to a standard turbidity of 0.5 McFarland. Bacteria were seeded in 150 mm × 15 mm Petri dishes containing Mueller-Hilton agar. Inhibitory activity was observed when a halo or zone of inhibition formed around the antimicrobial discs, inhibiting bacterial growth, and the diameter was measured in millimeters (mm) using a ruler.

Vibrational spectroscopy

Infrared spectra were obtained for the samples using a PerkinElmer brand Fourier-transform infrared (FTIR) spectrometer (Spectrum Two model). The region of analysis was set to 4,000–400 cm^{-1}, with a resolution of 4 cm^{-1}, and the average number of scans was 32. Raman measurements were performed using a Brucker RFS 100 spectrometer, which was equipped with a neodymium-doped yttrium aluminium garnet (Nd^{+3}/YAG) laser operating at a wavelength of 1,064 nm in the near-infrared range and a germanium detector that was cooled with liquid nitrogen. The instrument had a resolution of 4 cm^{-1}, with an average of 516 accumulations.

Micro-Raman image

The measurements were conducted using Brucker SENTERRA instrumentation model affixed to the microscope. The Raman image was obtained by mapping twenty points on the sample with the use of a 50× optical lens. The analysis parameters were as follows: laser excitation at 785 nm, an average of 25 co-additions, 3.0 seconds of exposure for each point, laser power of 10 mW, and a spectral resolution of 4 cm^{-1}.

Scanning electron microscopy

SEM images were obtained using a Hitachi Tabletop TM 3000 scanning electron microscope with magnification from 50× up to 10,000× with no sample preparation (no metallic recovery of the samples), a backscattered electron detector (BSE), and 15 keV observation condition mode.

Results

Table 2 summarizes film uniformity data in relation to mass, thickness, and MUP concentration. It was observed that all films presented uniformity in the three parameters analyzed, presenting a low standard deviation. However, there was a difference in thickness and uniformity between the films, with F2 presenting a greater thickness and thus a greater mass. Figure 2 depicts the bar graph of the absorptive capacity and the results of the two-way ANOVA analysis. The data were evaluated for normality using the Kolmogorov-Smirnov test, and the homogeneity of variance was assessed using the Bartlett test. In all statistical tests, a significance level of $p < 0.05$ was employed. The statistical analyses were conducted using GraphPad Prism software, version 7.0 for Windows (GraphPad Software).

Table 2. Parameters analyzed in the films

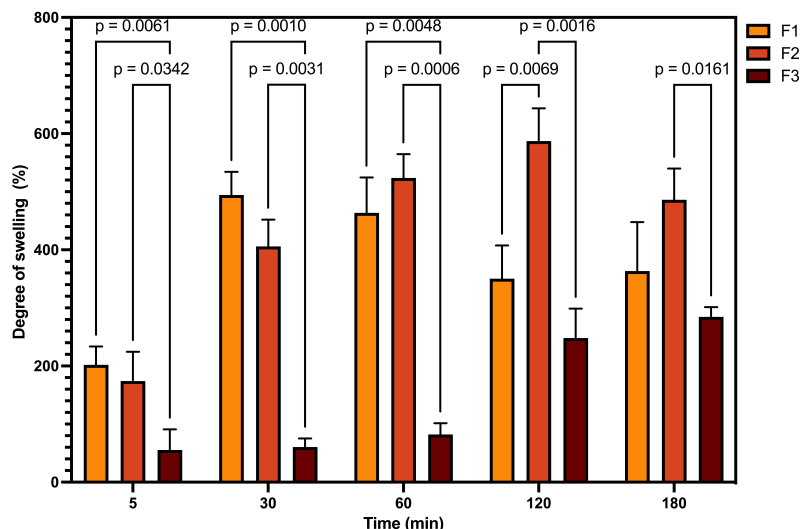| Films	Mass uniformity (g)	Thickness (mm)	MUP concentration (%)
F1	0.0055 ± 0.0012	0.1700 ± 0.0447	3.403 ± 0.2489
F2	0.0107 ± 0.0019	0.2800 ± 0.0758	3.602 ± 0.5039
F3	0.0057 ± 0.0012	0.1480 ± 0.0045	3.825 ± 0.1536

MUP: mupirocin

Figure 2. Illustrates the degree of absorption of the samples, together with the results of the two-way ANOVA analysis.
F1: 50% sodium alginate and 50% κ-carrageenan, crosslinked; F2: 75% sodium alginate and 25% κ-carrageenan, crosslinked; F3: 25% sodium alginate and 75% κ-carrageenan, crosslinked

Figure 3 shows the Raman spectra of MUP and the carbohydrates used to obtain the films, and Table 3 summarizes the attempt to assign bands [21–25]. Figure 4 presents the Raman spectra of the films obtained with and without crosslinking to compare and identify the spectral changes. Thus, in the film spectra, it was possible to observe bands at 359, 893, and 1,093 cm^{-1} and associate them with the presence of both carbohydrates. The bands at 736 and 853 cm^{-1} are related to κ-carrageenan and those at 809 and 957 cm^{-1} are related to sodium alginate.
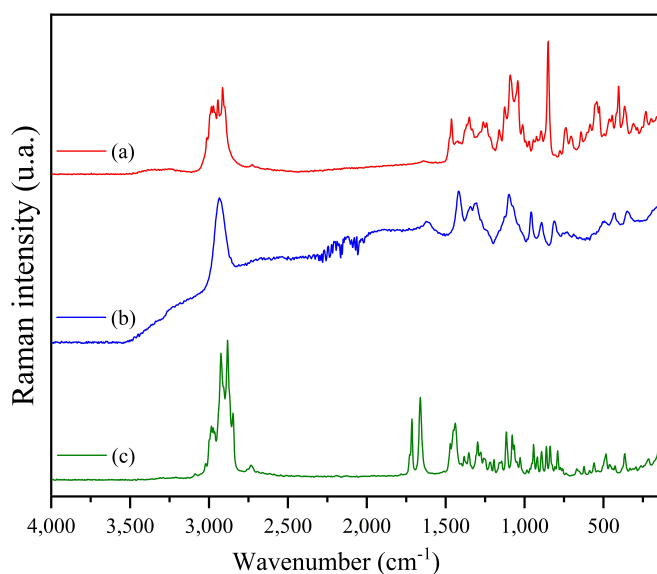

Figure 3. Raman spectra of κ-carrageenan (a), sodium alginate (b), and mupirocin (c)

Table 3. Tentative Raman bands assignment (cm^{-1})

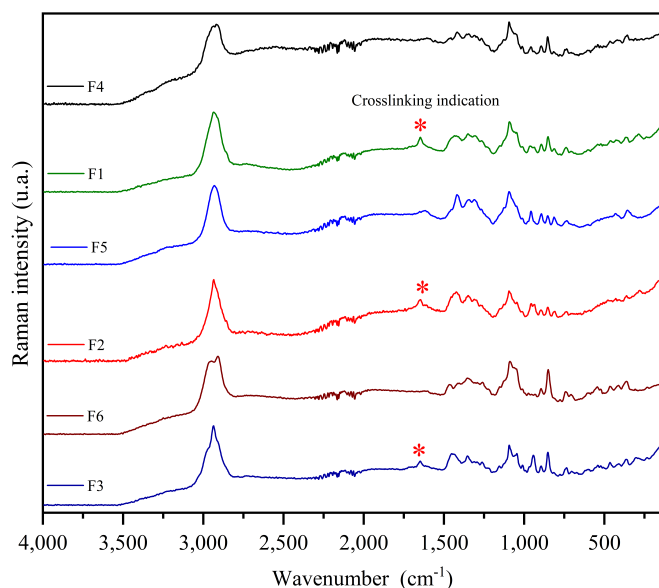| Sodium alginate	κ-carrageenan	Assignment
1,620/1,417		$v(COO^-)$
1,306/1,344		$\delta(CH)$
	1,258	$(S=O)$
1,100		Glycoside ring respiration
959		$\delta(C–C–H)$, $\delta(C–O–H)$ and $v(C–O–C)$
810		$\delta(C–O–H)$, $v(C–C)$, $v(C–O)$, $\delta(C–C–H)$ and $\delta(C–C–O)$
	1,090	$v(C–O)$
	848	$(C–O–SO_4)$
430		$\delta(C–C–C)$ and $\delta(C–O–C)$

Figure 4. Raman spectra of the films. F1: 50% sodium alginate and 50% κ-carrageenan, crosslinked; F2: 75% sodium alginate and 25% κ-carrageenan, crosslinked; F3: 25% sodium alginate and 75% κ-carrageenan, crosslinked; F4: 50% sodium alginate and 50% κ-carrageenan, non-crosslinked; F5: 75% sodium alginate and 25% κ-carrageenan, non-crosslinked; F6: 25% sodium alginate and 75% κ-carrageenan, non-crosslinked

Figure 5 presents the infrared spectra of MUP and the carbohydrates used to obtain the films, and Table 4 summarizes the assignment of the observed bands [25–33]. Figure 6 presents the infrared spectra of the films obtained with and without crosslinking to compare and identify the spectral changes. Bands associated with both carbohydrates were observed in the spectra of all samples.

Figure 7 presents the permeation data using the Franz cell and the polysulfone membrane in a medium of phosphate buffer and 5% methanol. First, MUP presents a good release for all films except for F3, as it was the only film with a permeation percentage lower than 60%. This may be related to the fact that the film presented lower degrees of swelling than the other films, which would lead to lower MUP release [1]. Furthermore, a controlled release process was observed in all films, as immediate permeation was not observed; this only occurred when MUP permeation was analyzed without the presence of polymeric film. To study the permeation and release kinetics, the data were fitted to zero-order, first-order, Higuchi, Peppas-Korsmeyer, and Weibull models. The equations for each model, parameters obtained, and statistical analyses for each film are summarized in Table 5.

Figure 8 shows the micro-Raman images of the κ-carrageenan/alginate films obtained by integrating the band at 864 cm^{-1}. This was chosen because it is a region where only κ-carrageenan shows a signal. In the Raman image of all the mixtures, 20 points were analyzed, and in all of them the presence of bands at 864 cm^{-1} was observed, with more or less intensity, represented by blue to red coloration on the contour map.
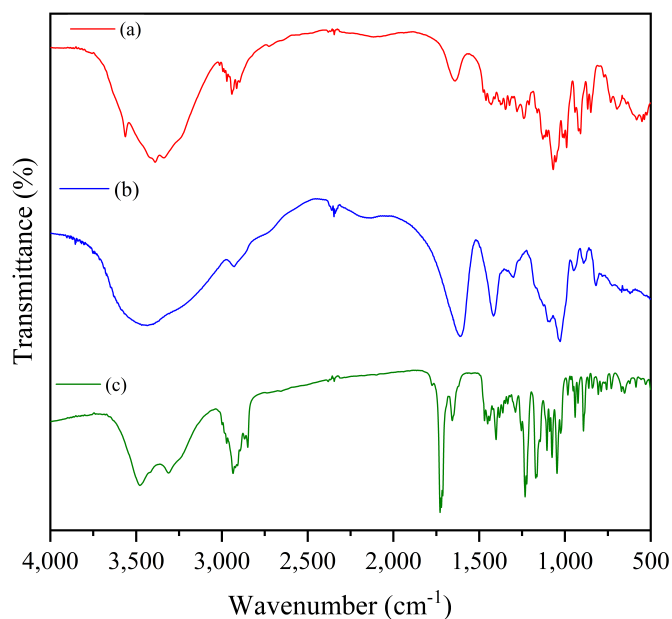
Figure 5. Infrared absorption spectra of κ-carrageenan (a), sodium alginate (b), and mupirocin (c)

Table 4. Tentative infrared bands assignment (cm^{-1})

Sodium alginate	κ-carrageenan	Assignment
3,443	3,600–3,100	(OH)
	3,100–2,800	(CH)
2,970		ν(OH)
	1,642	δ(OH)
1,610		$\nu_{asymmetric}$ (COO$^-$)
1,417		$\nu_{symmetric}$ (COO$^-$)
	1,238	ν(S=O)
1,258		ν(C–O)
1,165		ν(C–O), ν(C–C) and δ (C–C–C)
	912	ν(C–O–C) glycosidic bond
	848/704	δ(C–O–S)

Figure 9 shows SEM images of the films. The solvent evaporation method used in this study does not normally produce interesting architectural structures, such as electrospinning or phase separation methods [1, 34]. However, analysis using SEM can provide useful information on the miscibility of the polymers that form the film. Film F2 was the only film that presented a flat surface, as opposed to films F1 and F3, which presented an agglomerated surface after evaporation of the solvent. However, for all of them, phase separation was not observed.

Figure 10 depicts the bar graph representing the diameters of inhibition and the results of the one-way analysis of variance (adjusted *p*-value). The data were assessed for normality using the Kolmogorov-Smirnov test, and the homogeneity of variance was evaluated through the utilization of Bartlett's test. The impact of the samples on bacterial growth was evaluated through one-way analysis of variance (ANOVA), followed by a Tukey test. In all statistical tests, a significance level of $p < 0.05$ was employed. The statistical analyses were conducted using GraphPad Prism software, version 7.0 for Windows (GraphPad Software).

Discussion

The mechanical properties of a polymer are significantly influenced by the crosslinking density. The modulus or rigidity of polymers with a higher crosslinking density is typically enhanced [35]. In addition, polymer blends can change the properties of the system, such as the three-dimensional organization of the chains and, consequently, the thickness of the film [36]. In this context, the observed thicknesses of the
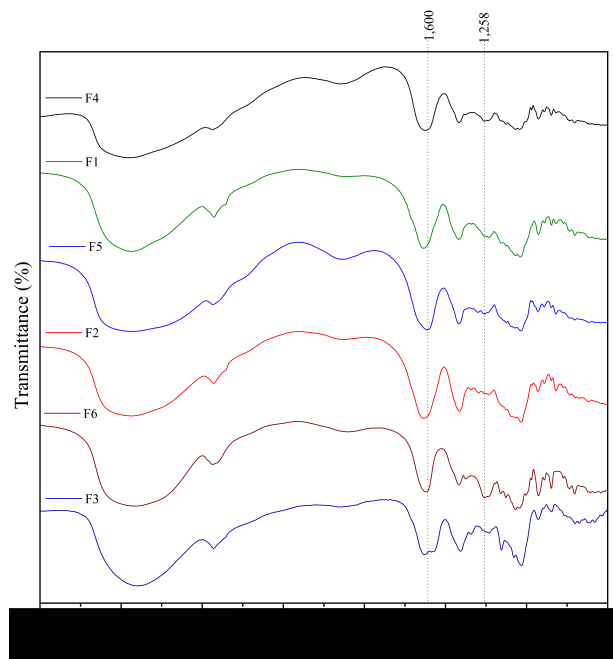
Figure 6. Infrared absorption spectra of the films. F1: 50% sodium alginate and 50% κ-carrageenan, crosslinked; F2: 75% sodium alginate and 25% κ-carrageenan, crosslinked; F3: 25% sodium alginate and 75% κ-carrageenan, crosslinked; F4: 50% sodium alginate and 50% κ-carrageenan, non-crosslinked; F5: 75% sodium alginate and 25% κ-carrageenan, non-crosslinked; F6: 25% sodium alginate and 75% κ-carrageenan, non-crosslinked
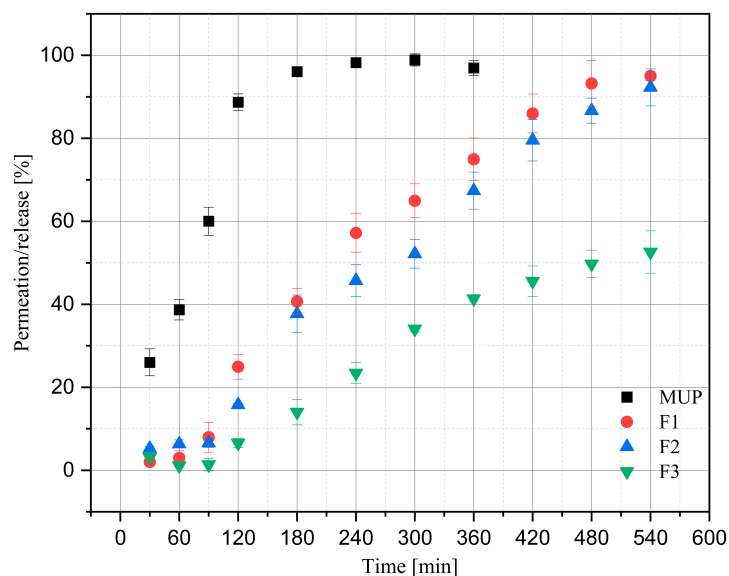

Figure 7. Graph of film permeation/release profiles. MUP: mupirocin; F1: 50% sodium alginate and 50% κ-carrageenan, crosslinked; F2: 75% sodium alginate and 25% κ-carrageenan, crosslinked; F3: 25% sodium alginate and 75% κ-carrageenan, crosslinked. The release of MUP was conducted until the time of 360 minutes, as it was observed that after 240 minutes there was a stabilization of concentration

polymeric films can be attributed to the distinct proportions of carbohydrates utilized in each film and the potential for varying degrees of crosslinking, given the disparate compositions of each film. Regarding the MUP concentration, it is observed that the films present values between 3.403 and 3.825%; however, these values are lower than the 8.0% added during the preparation of the polymeric film. This may be due to the non-total solubilization of MUP and its deposition in the Petri dish and/or the crosslinking and washing process that resulted in the MUP leaching process.

The swelling capacity of polymeric films is an important parameter when applied to dressings. Carbohydrates, such as carrageenan and sodium alginate, swell in physiological fluids [37, 38]. The water absorption capacity and rate of crosslinked and water swellable polymers can be explained in terms of the diffusion of water in the polymer network and the dynamics of hydrogen bond formation. Consequently, as

Table 5. Data referring to kinetic models

Models[※]	Parameters	MUP	F1	F2	F3
Zero-order	k_0	0.0026	0.0189	0.0108	0.0068
$Q_t = Q_0 + k_0 t$	R^2	0.9480	0.9776	0.9626	0.9951
First-order	k_1	0.0551	0.0024	0.0042	0.0042
$LogQ_t = LogQ_0 + \dfrac{k_1 t}{2.203}$	R^2	0.5730	0.657	0.8805	0.5359
Higuchi	k_H	0.0444	0.0169	0.0143	0.0131
$\dfrac{M_t}{M_\infty} = k_H t^{1/2}$	R^2	0.9315	0.6359	0.5677	0.8585
	χ^2	5.774	94.47	151.2	4,206
Peppas-Korsmeyer	k	0.0201	0.001	4.775×10^{-4}	7.086×10^{-5}
$\dfrac{M_t}{M_\infty} = k t^n$	n	0.7070	1.087	1.215	1.470
	R^2	0.9662	0.9853	0.9622	0.9826
	χ^2	2.8275	9.874	7.138	9.757
Weibull	T_0	8.188	8.822	10.77	8.7978
$\dfrac{M_t}{M_\infty} = 1 - e^{-\left(\frac{t - T_0}{\tau}\right)^\beta}$	τ	111.0	269.4	316.2	517.6
	β	1.006	1.623	1.665	1.683
	R^2	0.9776	0.9984	0.9949	0.9904
	χ^2	2.155	1.345	1.578	4.509

[※] Zero-order: Q_t represents the quantity of drug dissolved over time t, with Q_0 denoting the initial amount of drug present in the solution and k_0 is the zero-order release constant, expressed in units of concentration per time. First-order: Q_t represents the quantity of drug dissolved over time t, with Q_0 denoting the initial amount of drug present in the solution, and k_1 is the first-order rate constant. Higuchi: M_t is the amount of drug released over time t, M_∞ is the amount of drug released after time ∞, and k_H represents the Higuchi release kinetic constant. Peppas-Korsmeyer: M_t/M_∞ is the fraction of drug released at the time t, k is the release rate constant, and n is the release exponent. Weibull: M_t is the amount of drug dissolved as a function of time t, M_∞ is the total amount of drug released, T_0 accounts for the lag time measured due to the dissolution process, τ denotes a scale parameter describing the time dependence, and β describes the shape of the dissolution curve progression. MUP: mupirocin; F1: 50% sodium alginate and 50% κ-carrageenan, crosslinked; F2: 75% sodium alginate and 25% κ-carrageenan, crosslinked; F3: 25% sodium alginate and 75% κ-carrageenan, crosslinked

the crosslinking density is responsible for forming the 3D structure of the materials, it will influence the water absorption process [39]. Thus, if the degree of crosslinking is insufficient, the interactions between the polymer chains will be readily disrupted, resulting in a fragile hydrogel that is susceptible to dissolution in water. Conversely, a high degree of crosslinking will result in a reduction in the hydrogel's swelling capacity [40]. A statistical comparison of the samples reveals that films F1 and F2 exhibit comparable absorption capacity, exceeding that of sample F3. Additionally, mass loss is discernible in samples F1 and F2 after 120 and 180 minutes, respectively, whereas this phenomenon is not observed in film F3. This may be associated with the elevated proportion of κ-carrageenan in the film F3 and a greater degree of crosslinking.

The crosslinking process can be confirmed by comparing the Raman spectra of the films with and without crosslinking; thus, the appearance of a band at 1,650 cm^{-1} is observed, which can be associated with the interaction of the alginate carboxylic group with Zn^{2+} ions. It was also observed that the band at 956 cm^{-1} split into two in the spectra of the crosslinked films (F1 and F2) compared to the spectrum of the non-crosslinked films; for the F3 crosslinked film, this band was not present in the spectrum of the non-crosslinked film. As this band is associated only with sodium alginate and attributed to δ(C–O–H), it can indicate the interaction process between the Zn^{2+} ions and the alginate hydroxyl. This result corresponds with the literature, which describes the formation of a complex between this carbohydrate and Zn^{2+} ions [41]. In relation to κ-carrageenan, it is not possible to indicate the crosslinking process from the Raman spectra, because it would occur owing to the interaction of the OSO$_3^-$ groups with Zn^{2+} and the band related to (S=O) appears superimposed on sodium alginate bands. However, the literature describes the formation and interaction of the carrageenan complex with Zn^{2+} [42, 43].

Regarding infrared, some changes indicated crosslinking through Zn^{2+} ions. The carbonyl stretches of sodium alginate (approximately 1,600 cm^{-1}) shifted to higher wavenumbers after crosslinking, which may be related to the formation of coordinated bonds between the carboxylate groups of alginate and Zn^{2+} ions.
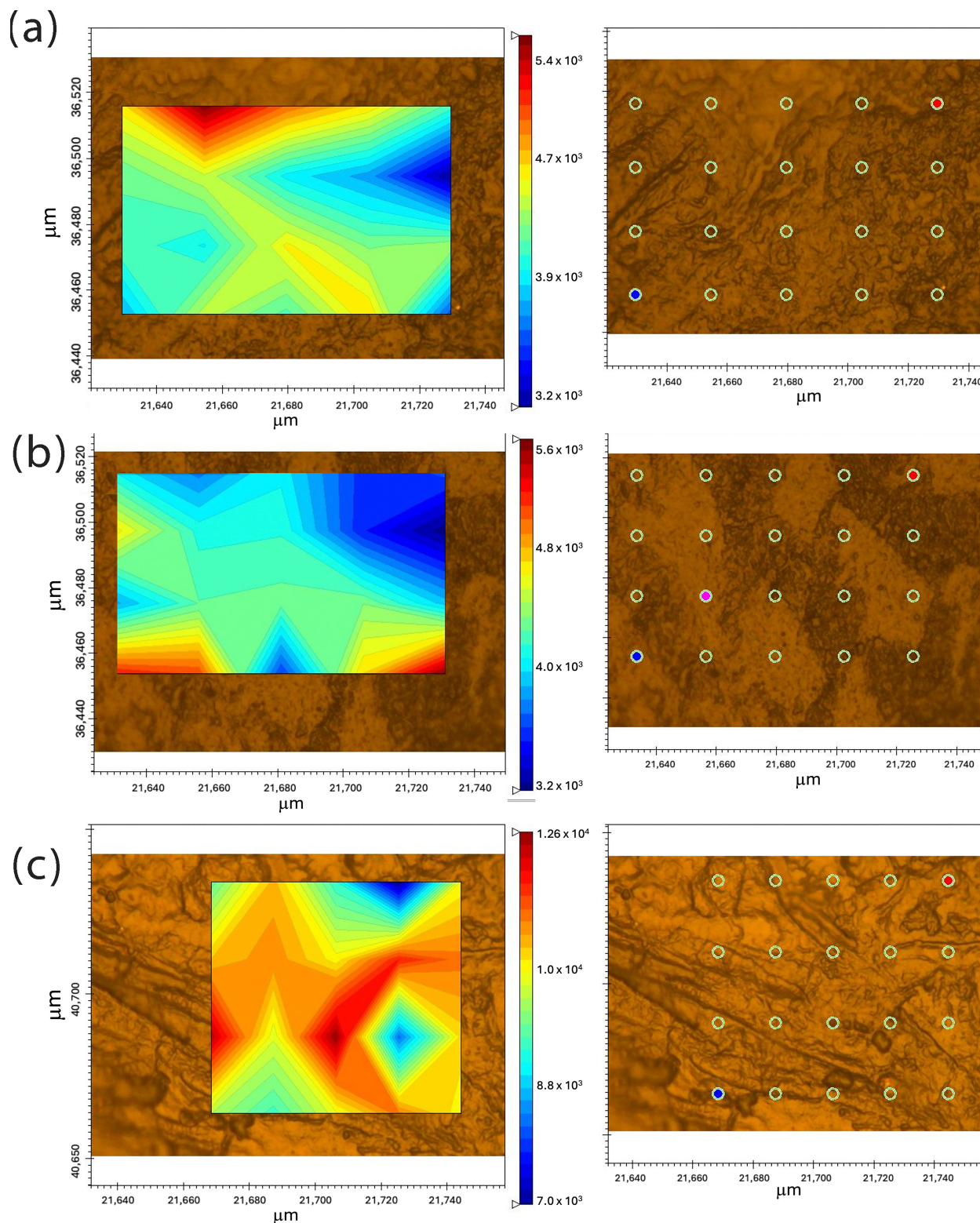
Figure 8. Micro-Raman image of films. F1: 50% sodium alginate and 50% κ-carrageenan, crosslinked; F2: 75% sodium alginate and 25% κ-carrageenan, crosslinked; F3: 25% sodium alginate and 75% κ-carrageenan, crosslinked

This is because coordination changes the length of the C=O bond, which produces a change in wavenumbers [43]. In relation to the carbonyl group of the F3 film, the band at 1,417 cm^{-1} shifted to lower wavenumbers, indicating the possibility of an interaction between this chemical group and Zn^{2+}. In relation to κ-carrageenan, one of the likely interactions with Zn^{2+} would be with the sulfonic group, which would alter the bands at 1,258, 848, and 704 cm^{-1}. In relation to the band at 1,258 cm^{-1}, a decrease in its relative intensity is observed after crosslinking. For the bands at 704 and 848 cm^{-1}, it is not possible to observe any change. However, in the literature, it is described that the interaction between ʎ-carrageenan and Zn^{2+}
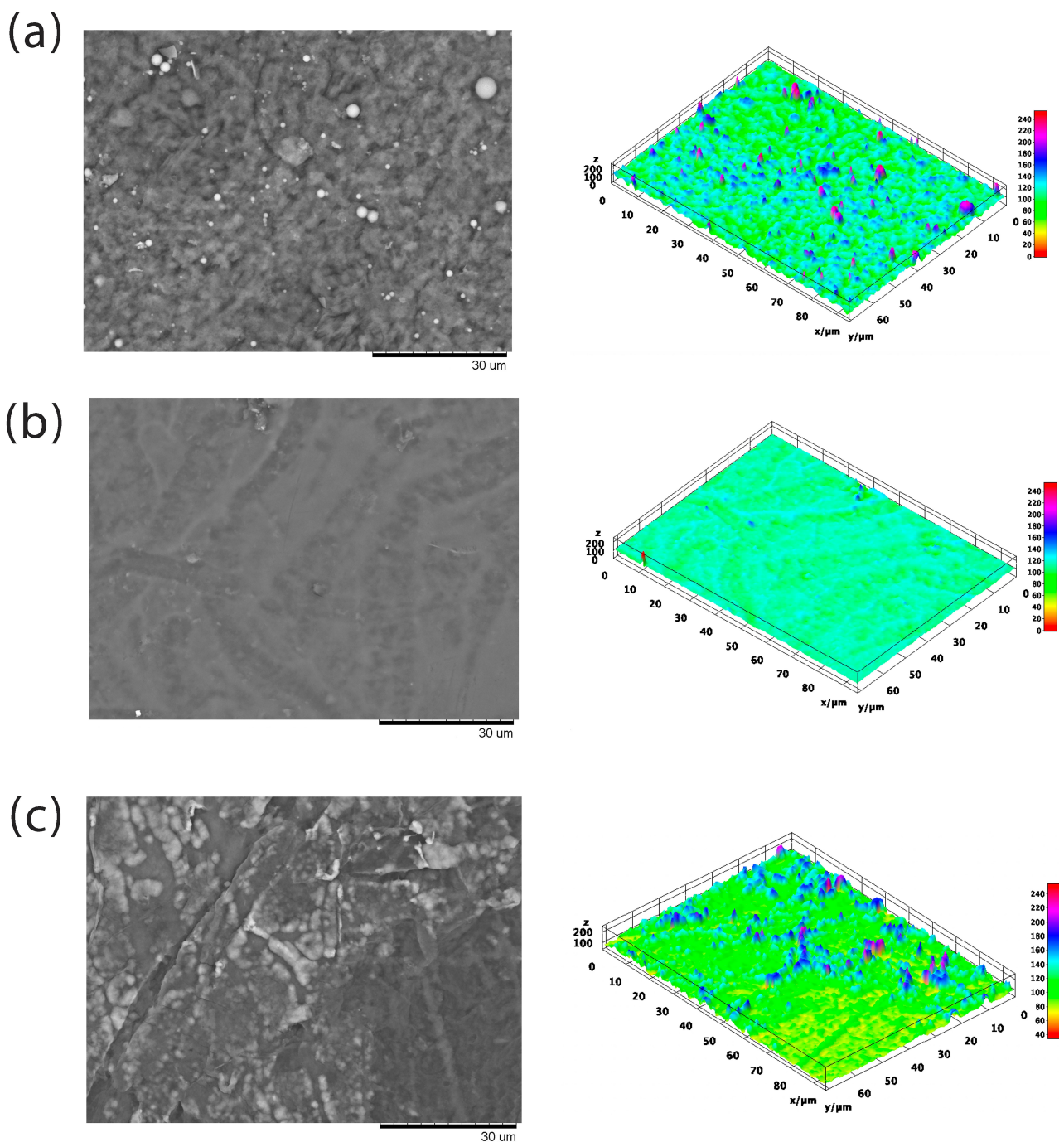
Figure 9. Scanning electron microscopy of films. F1: 50% sodium alginate and 50% κ-carrageenan, crosslinked; F2: 75% sodium alginate and 25% κ-carrageenan, crosslinked; F3: 25% sodium alginate and 75% κ-carrageenan, crosslinked

shifts the band at 1,258 cm^{-1} to lower wave numbers; thus, it is possible to assume that the change observed in the present study also indicates this interaction [43].

The utilization of polymeric films for the regulated release of MUP has been the subject of numerous investigations. The permeation flow of films comprising high and low molecular weight chitosan was investigated using rabbit skin, and it was demonstrated that the sustained drug release effect could be maintained for up to 24 hours [44, 45]. The same period of controlled release was achieved using rabbit skin in hydrogels composed of acrylic acid and 2-acrylamido-2-methylpropane sulfonic acid. The in vitro release study of compounds containing chitosan, sodium alginate and Carbopol® showed that MUP release was enhanced, with maximum release occurring at 12 h [46]. The release duration observed in this study was up to nine hours, a value that falls below that reported in comparable studies. However, it is important to note that the studies used rabbit skin as the membrane, which will inherently have a reduced release profile compared to a synthetic membrane [47].
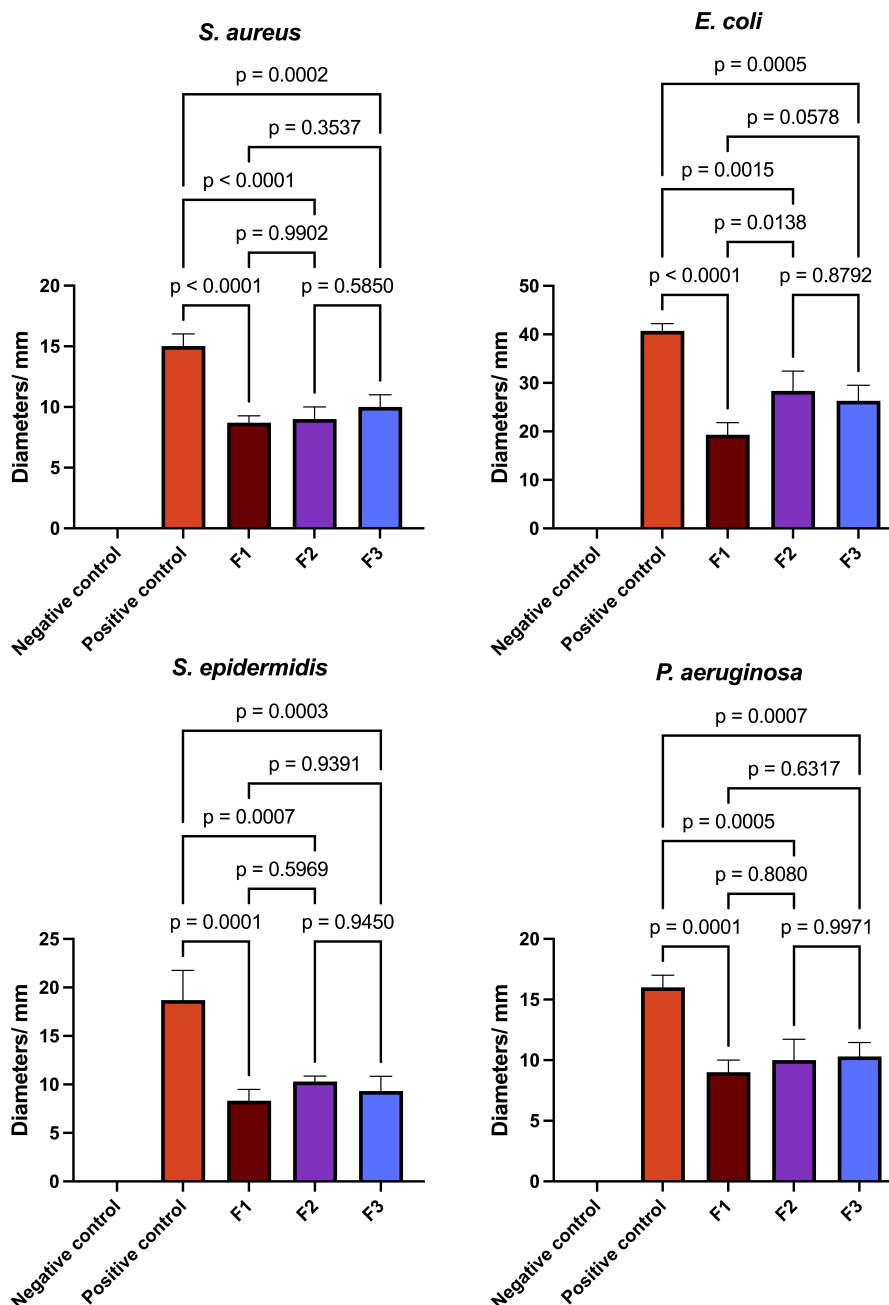
Figure 10. The data presented in bar graphs illustrates the diameters of inhibition, and one-way ANOVA analysis. F1: 50% sodium alginate and 50% κ-carrageenan, crosslinked; F2: 75% sodium alginate and 25% κ-carrageenan, crosslinked; F3: 25% sodium alginate and 75% κ-carrageenan, crosslinked

In relation to the release kinetics models studied, it was observed that the Higuchi model did not fit well with the experimental data on the permeation of polymeric films, as it presented lower coefficients of determination. This can be explained by the fact that the polymeric films exhibit a high degree of swelling, which was not predicted by this model [48]. However, this model applies well to MUP permeation without polymeric films, because swelling does not occur. The polymeric and MUP films also fit the zero-order model because the coefficient of determination was close to 1.0. This indicated that the permeation and release processes were slow [49]. The Peppas-Korsmeyer model, all the samples presented a coefficient of determination close to 1.0, indicating a good fit with the experimental data. For polymeric films, all values of n were greater than 0.89, indicating that the mechanism of super-relaxation of polymeric chains is decisive for the release and permeation of MUP; however, for MUP permeation, the value of n was 0.7070, indicating non-Fickian transport [19]. The Weibull model, a good fit of the experimental data was also observed; therefore, it was possible to analyze parameter T_0, which presented values close to 10 min in all

experiments. This may indicate that the polymeric films have MUP on their surface, which is immediately released; this is why the T_0 values of the films and isolated MUP are approximately equal [19].

Polymer blends often exhibit compositional and morphological heterogeneity that affects the overall properties of the material. Therefore, it is possible to better understand the influence of heterogeneity on material properties by obtaining a high-resolution spatial distribution of the components of a sample composed of different polymers. In this context, the spatial distribution of molecular species in polymer mixtures can be studied using micro-Raman image analysis [50]. The results demonstrate the presence of κ-carrageenan in all points of the sample, as well as homogeneity at a spatial resolution of approximately 1 μm. This may indicate the presence of similar properties in the different areas of the samples [51]. Similarly, the data obtained by SEM do not indicate the presence of phase separation in the samples.

Regarding microbiological tests, it can be observed that the positive control demonstrated a more pronounced inhibitory effect on all bacterial strains, with a statistically significant difference between the various films ($p < 0.05$). With respect to the polymeric films, the results for *S. aureus*, *S. epidermidis*, and *P. aeruginosa* were comparable, as evidenced by an adjusted *p*-value exceeding 0.05 in all comparisons. Regarding the inhibitory activities on *E. coli*, it can be observed that the F2 and F3 films show comparable inhibitory effects and more pronounced than those observed in the F1 sample. Similar findings have been previously documented in the scientific literature. Films composed of chitosan, sodium alginate, and Carbopol® loaded with MUP demonstrated antimicrobial activity against a range of bacteria, including *E. coli* (ATCC 8739), *Enterococcus hirae* (ATCC 10541), *S. aureus* (ATCC 6538), *P. aeruginosa* (ATCC 27853), *Bacillus cereus* (ATCC 7064), and *Klebsiella pneumoniae* [1].

Conclusions

These results demonstrate the potential of using κ-carrageenan and sodium alginate for the development of polymeric films for the controlled delivery of MUP, aimed at the production of dressings that can improve wound treatment. Vibrational spectroscopy data (infrared and Raman) indicated the presence of both carbohydrates in the polymeric films and the interactions between the Zn^{2+} ions and the carbohydrates, which resulted in the crosslinking process. The films exhibited good uniformity in terms of mass, thickness, and concentration of MUP; however, the percentage of antibiotics present in the films was lower than that added, indicating loss during the crosslinking and washing processes of the films. The films exhibited good swelling; however, over time, the swelling decreased, probably owing to erosion or another mechanism. In vitro antibiotic permeation/release studies demonstrated the controlled release of the drug, which was almost completely dissolved in films F1 and F2. The morphology of the films was studied using micro-Raman imaging and SEM; the first technique demonstrated a homogeneous distribution of carbohydrates in the films, without indicating the formation of phases, and the second technique also indicated the non-formation of different phases and the formation of mostly flat surfaces. The films exhibited good activity against *S. aureus*, *E. coli*, *S. epidermidis*, and *P. aeruginosa*; however, the F2 film exhibited the best formal activity. The findings suggest that the utilization of films as a matrix for the controlled release of MUP may prove beneficial for wound treatment. Formulation F2 was identified as the most suitable for film production as it has a higher percentage of MUP release and more pronounced antimicrobial activity against *E. coli*.

Abbreviations

ATCC: American Type Collection Culture

F1: 50% sodium alginate and 50% κ-carrageenan, crosslinked

F2: 75% sodium alginate and 25% κ-carrageenan, crosslinked

F3: 25% sodium alginate and 75% κ-carrageenan, crosslinked

F4: 50% sodium alginate and 50% κ-carrageenan, non-crosslinked

F5: 75% sodium alginate and 25% κ-carrageenan, non-crosslinked

F6: 25% sodium alginate and 75% κ-carrageenan, non-crosslinked

MUP: mupirocin

SEM: scanning electron microscopy

UV-vis: ultraviolet-visible

Declarations

Author contributions

TRdS: Conceptualization, Investigation, Writing—original draft. SDdS: Investigation. GSC: Conceptualization, Investigation, Writing—original draft. NLGDdS: Conceptualization, Investigation, Writing—original draft, Supervision, Writing—review & editing. All authors read and approved the submitted version.

Conflicts of interest

The authors declare that they have no conflicts of interest.

Ethical approval

Not applicable.

Consent to participate

Not applicable.

Consent to publication

Not applicable.

Availability of data and materials

The raw data supporting the conclusions of this manuscript is available upon inquiry at nelson.luis@uft.edu.br without undue reservation, by any qualified researcher.

Publisher's note

Open Exploration maintains a neutral stance on jurisdictional claims in published institutional affiliations and maps. All opinions expressed in this article are the personal views of the author(s) and do not represent the stance of the editorial team or the publisher.

References

1. Üstündağ Okur N, Hökenek N, Okur ME, Ayla Ş, Yoltaş A, Siafaka PI, et al. An alternative approach to wound healing field; new composite films from natural polymers for mupirocin dermal delivery. Saudi Pharm J. 2019;27:738–52. [DOI]

2. Fráguas RM, Rocha DA, de Rezende Queiroz E, de Abreu CMP, de Sousa RV, Oliveira Júnior EN. Chemical characterization and healing effect of chitosan with low molar mass and acetylation degree in skin lesions. Polímeros. 2015;25:205–11. [DOI]

3. Mihai MM, Preda M, Lungu I, Gestal MC, Popa MI, Holban AM. Nanocoatings for Chronic Wound Repair-Modulation of Microbial Colonization and Biofilm Formation. Int J Mol Sci. 2018;19:1179. [DOI] [PubMed] [PMC]

4. Santos VLCG, Oliveira ADS, Amaral AFDS, Nishi ET, Junqueira JB. Quality of life in patients with chronic wounds: magnitude of changes and predictive factors. Rev Esc Enferm USP. 2017;51:e03250. [DOI] [PubMed]

5. Soares Dantas J, Silva CCM, Nogueira WP, de Oliveira E Silva AC, de Araújo EMNF, da Silva Araújo P, et al. Health-related quality of life predictors in people with chronic wounds. J Tissue Viability. 2022;31: 741–5. [DOI] [PubMed]

6. de Oliveira AC, de Macêdo Rocha D, Bezerra SMG, Andrade EMLR, dos Santos AMR, Nogueira LT. Quality of life of people with chronic wounds. Acta Paulista de Enfermagem. 2019;32:194–201. [DOI]

7. Mpharm KD, Ramana MV, Sara UVS, Agrawal DK, Mpharm KP, Chakravarthi S. Preparation and evaluation of transdermal plasters containing norfloxacin: a novel treatment for burn wound healing. Eplasty. 2010;10:e44. [PubMed] [PMC]

8. Shende MA, Sayyad HG. Development and Validation of Spectroscopic Analytical Method for Simultaneous Estimation of Mupirocin and Satranidazole in Bulk and Topical Formulation. Int J Pharm Pharm Res. 2017;10:225–40.

9. Lamb YJ. Overview of the role of mupirocin. J Hosp Infect. 1991;19:27–30. [DOI] [PubMed]

10. Gangwar A, Kumar P, Singh R, Kush P. Recent Advances in Mupirocin Delivery Strategies for the Treatment of Bacterial Skin and Soft Tissue Infection. Future Pharmacol. 2021;1:80–103. [DOI]

11. Tran TTD, Tran PHL. Controlled Release Film Forming Systems in Drug Delivery: The Potential for Efficient Drug Delivery. Pharmaceutics. 2019;11:290. [DOI] [PubMed] [PMC]

12. Yasasvini S, Anusa RS, VedhaHari BN, Prabhu PC, RamyaDevi D. Topical hydrogel matrix loaded with Simvastatin microparticles for enhanced wound healing activity. Mater Sci Eng C Mater Biol Appl. 2017;72:160–7. [DOI] [PubMed]

13. Deng H, Yu Z, Chen S, Fei L, Sha Q, Zhou N, et al. Facile and eco-friendly fabrication of polysaccharides-based nanocomposite hydrogel for photothermal treatment of wound infection. Carbohydr Polym. 2020;230:115565. [DOI] [PubMed]

14. Far BF, Naimi-Jamal MR, Safaei M, Zarei K, Moradi M, Nezhad HY. A Review on Biomedical Application of Polysaccharide-Based Hydrogels with a Focus on Drug Delivery Systems. Polymers (Basel). 2022; 14:5432. [DOI] [PubMed] [PMC]

15. Koga AY, Felix JC, Silvestre RGM, Lipinski LC, Carletto B, Kawahara FA, et al. Evaluation of wound healing effect of alginate film containing Aloe vera gel and cross-linked with zinc chloride. Acta Cir Bras. 2020;35:e202000507. [DOI] [PubMed] [PMC]

16. Priyadarshi R, Sauraj, Kumar B, Negi YS. Chitosan film incorporated with citric acid and glycerol as an active packaging material for extension of green chilli shelf life. Carbohydr Polym. 2018;195:329–38. [DOI] [PubMed]

17. Laracuente M, Yu MH, McHugh KJ. Zero-order drug delivery: State of the art and future prospects. J Control Release. 2020;327:834–56. [DOI] [PubMed]

18. Trucillo P. Drug Carriers: A Review on the Most Used Mathematical Models for Drug Release. Processes. 2022;10:1094. [DOI]

19. Dash S, Murthy PN, Nath L, Chowdhury P. Kinetic modeling on drug release from controlled drug delivery systems. Acta Pol Pharm. 2010;67:217–23. [PubMed]

20. Gajic I, Kabic J, Kekic D, Jovicevic M, Milenkovic M, Culafic DM, et al. Antimicrobial Susceptibility Testing: A Comprehensive Review of Currently Used Methods. Antibiotics (Basel). 2022;11:427. [DOI] [PubMed] [PMC]

21. Schmid T, Messmer A, Yeo B, Zhang W, Zenobi R. Towards chemical analysis of nanostructures in biofilms II: tip-enhanced Raman spectroscopy of alginates. Anal Bioanal Chem. 2008;391:1907–16. [DOI] [PubMed]

22. Campos-Vallette MM, Chandía NP, Clavijo E, Leal D, Matsuhiro B, Osorio-Román IO, et al. Characterization of sodium alginate and its block fractions by surface-enhanced Raman spectroscopy. J Raman Spectrosc. 2010;41:758–63. [DOI]

23. Cazzolli G, Caponi S, Defant A, Gambi CMC, Marchetti S, Mattarelli M, et al. Aggregation processes in micellar solutions: a Raman study. J Raman Spectrosc. 2012;43:1877–83. [DOI]

24. Mahardika A, Susanto AB, Pramesti R, Matsuyoshi H, Andriana BB, Matsuda Y, et al. Application of imaging Raman spectroscopy to study the distribution of *Kappa* carrageenan in the seaweed *Kappaphycus alvarezii*. J Appl Phycol. 2018;31:1383–90. [DOI]

25. Carmo IAD, de Souza AKN, Fayer L, Munk M, de Mello Brandão H, de Oliveira LFC, et al. Cytotoxicity and bactericidal activity of alginate/polyethylene glycol films with zinc oxide or silicon oxide nanoparticles for food packaging. Int J Polym Mater Polym Biomater. 2023;72:577–88. [DOI]

26. Sartori C, Finch DS, Ralph B, Gilding K. Determination of the cation content of alginate thin films by *FT*i.r. spectroscopy. Polymer. 1997;38:43–51. [DOI]

27. Bojarska J, Maniukiewicz W, Fruziński A, Jędrzejczyk M, Wojciechowski J, Krawczyk H. Structural and spectroscopic characterization and Hirshfeld surface analysis of major component of antibiotic mupirocin – pseudomonic acid A. J Mol Struct. 2014;1076:126–35. [DOI]

28. Elsupikhe RF, Shameli K, Ahmad MB, Ibrahim NA, Zainudin N. Green sonochemical synthesis of silver nanoparticles at varying concentrations of κ-carrageenan. Nanoscale Res Lett. 2015;10:916. [DOI] [PubMed] [PMC]

29. Król Ż, Malik M, Marycz K, Jarmoluk A. Characteristic of Gelatine, Carrageenan and Sodium Alginate Hydrosols Treated by Direct Electric Current. Polymers. 2016;8:275. [DOI] [PubMed] [PMC]

30. Belattmania Z, Kaidi S, Atouani SE, Katif C, Bentiss F, Jama C, et al. Isolation and FTIR-ATR and ^{1}H NMR Characterization of Alginates from the Main Alginophyte Species of the Atlantic Coast of Morocco. Molecules. 2020;25:4335. [DOI] [PubMed] [PMC]

31. Kondolot Solak E, Kaya S, Asman G. Preparation, characterization, and antibacterial properties of biocompatible material for wound healing. J Macromol Sci Part A. 2021;58:709–16. [DOI]

32. Pereira R, Tojeira A, Vaz DC, Mendes A, Bártolo P. Preparation and Characterization of Films Based on Alginate and Aloe Vera. Int J Polym Anal Charact. 2011;16:449–64. [DOI]

33. van Hoogmoed CG, Busscher HJ, de Vos P. Fourier transform infrared spectroscopy studies of alginate-PLL capsules with varying compositions. J Biomed Mater Res A. 2003;67:172–8. [DOI] [PubMed]

34. Ghosal K, Chandra A, G P, S S, Roy S, Agatemor C, et al. Electrospinning over Solvent Casting: Tuning of Mechanical Properties of Membranes. Sci Rep. 2018;8:5058. [DOI] [PubMed] [PMC]

35. Mane ST, Ponrathnam S, Chavan N. Effect of Chemical Cross-linking on Properties of Polymer Microbeads: A Review. Can Chem Trans. 2016;3:473–85. [DOI]

36. Xue L, Zhang J, Han Y. Phase separation induced ordered patterns in thin polymer blend films. Prog Polym Sci. 2012;37:564–94. [DOI]

37. Huang MH, Yang MC. Swelling and biocompatibility of sodium alginate/poly(γ-glutamic acid) hydrogels. Polym Adv Technol. 2010;21:561–7. [DOI]

38. Wurm F, Lerchster N, Pinggera G, Pham T, Bechtold T. Swelling of kappa carrageenan hydrogels in simulated body fluid for hypothetical vessel occlusion applications. J Biomater Appl. 2022;37:588–99. [DOI] [PubMed] [PMC]

39. Wu Y, Joseph S, Aluru NR. Effect of cross-linking on the diffusion of water, ions, and small molecules in hydrogels. J Phys Chem B. 2009;113:3512–20. [DOI] [PubMed]

40. Nasution H, Harahap H, Dalimunthe NF, Ginting MHS, Jaafar M, Tan OOH, et al. Hydrogel and Effects of Crosslinking Agent on Cellulose-Based Hydrogels: A Review. Gels. 2022;8:568. [DOI] [PubMed] [PMC]

41. Fuks L, Filipiuk D, Majdan M. Transition metal complexes with alginate biosorbent. J Mol Struct. 2006; 792–793:104–9. [DOI]

42. Ariño C, Nadal AM, Esteban M, Casassas E. Voltammetric study of zinc(II) and lead(II) ions in the presence of alginate and pectin. Electroanalysis. 1992;4:757–64. [DOI]

43. Keshavarzipour F, Tavakol H. Zinc cation supported on carrageenan magnetic nanoparticles: A novel, green and efficient catalytic system for one-pot three-component synthesis of quinoline derivatives. Appl Organom Chem. 2017;31:e3682. [DOI]

44. Ahmad S, Minhas MU, Ahmad M, Sohail M, Abdullah O, Badshah SF. Preparation and Evaluation of Skin Wound Healing Chitosan-Based Hydrogel Membranes. AAPS PharmSciTech. 2018;19:3199–209. [DOI] [PubMed]

45. Ahmad S, Minhas MU, Ahmad M, Sohail M, Khalid Q, Abdullah O. Synthesis and evaluation of topical hydrogel membranes; a novel approach to treat skin disorders. J Mater Sci Mater Med. 2018;29:191. [DOI] [PubMed]

46. Ahmad S, Usman Minhas M, Ahmad M, Sohail M, Abdullah O, Khan KU. Topical hydrogel patches of vinyl monomers containing mupirocin for skin injuries: Synthesis and evaluation. Adv Polym Tech. 2018;37:3401–11. [DOI]

47. Neupane R, Boddu SHS, Renukuntla J, Babu RJ, Tiwari AK. Alternatives to Biological Skin in Permeation Studies: Current Trends and Possibilities. Pharmaceutics. 2020;12:152. [DOI] [PubMed] [PMC]

48. Siepmann J, Peppas NA. Higuchi equation: derivation, applications, use and misuse. Int J Pharm. 2011; 418:6–12. [DOI] [PubMed]

49. Salamanca CH, Barrera-Ocampo A, Lasso JC, Camacho N, Yarce CJ. Franz Diffusion Cell Approach for Pre-Formulation Characterisation of Ketoprofen Semi-Solid Dosage Forms. Pharmaceutics. 2018;10: 148. [DOI] [PubMed] [PMC]

50. Souza NLGD, Brandão HM, de Oliveira LFC. Chitosan and Poly(Methyl Methacrylate-Co-Butyl Methacrylate) Bioblends: A Compatibility Study. Polym Plast Technol Eng. 2014;53:319–26. [DOI]

51. Shirahase T, Komatsu Y, Tominaga Y, Asai S, Sumita M. Miscibility and hydrolytic degradation in alkaline solution of poly(L-lactide) and poly(methyl methacrylate) blends. Polymer. 2006;47: 4839–44. [DOI]